TECHNICAL NOTE

D-857

CONSTANT DENSITY APPROXIMATIONS FOR THE FLOW BEHIND AXISYMMETRIC SHOCK WAVES

By Albert G. Munson

Ames Research Center
Moffett Field, Calif.

NATIONAL AERONAUTICS AND SPACE ADMINISTRATION

WASHINGTON

May 1961

NATIONAL AERONAUTICS AND SPACE ADMINISTRATION

TECHNICAL NOTE D-857

CONSTANT DENSITY APPROXIMATIONS FOR THE FLOW BEHIND AXISYMMETRIC SHOCK WAVES

By Albert G. Munson

SUMMARY

The incompressible rotational flow equations are used to obtain solutions for the flow behind axisymmetric shock waves with conic longitudinal sections. The nonlinear part of the term due to rotation is retained in the analysis. Numerical results for standoff distance and stagnation point velocity gradient are presented for the case in which the shock wave is a paraboloid, a sphere, or an oblate or prolate ellipsoid. A similarity parameter is proposed which correlates approximately the flow behind geometrically similar shock waves at different free-stream conditions.

INTRODUCTION

Recently, high-speed computers have been used to great advantage in the solution of the supersonic blunt-body problem. The existing methods employ either the direct approach (i.e., given a body, the shock wave is calculated), reference 1, or the indirect approach (i.e., given a shock wave, the body is computed), references 2, 3, 4, and 5. The predictions of these theories have been compared with experiment, and results for standoff distance and body shape (or shock-wave shape) are in good agreement with the observed values. These methods do, however, suffer from the disadvantage that a new calculation must be made for every free-stream condition. It therefore seems desirable to obtain approximate analytical solutions to the problem which would provide simpler (though less accurate) results. These results might be useful in their own right and might also aid in the interpretation of the more exact numerical solutions.

The density ratio across a shock wave becomes very large at high supersonic Mach numbers and for ratios of specific heats near 1 ($c_p/c_v = \gamma \approx 1$). The subsequent deceleration of the flow to zero velocity at the stagnation point can, therefore, change the density only slightly. This fact has led several investigators to solve the inviscid incompressible rotational flow equations, imposing the exact boundary conditions behind the shock wave. Lighthill (ref. 6) has used this technique in the strong shock approximation to obtain a solution for the flow behind a spherical shock wave. Hida (ref. 7) earlier obtained a solution for the flow near

the axis. He did, however, consider all supersonic Mach numbers. Whitham (ref. 8), Hayes (ref. 9), and Hida have obtained the corresponding solution for flow behind a circular shock wave in two dimensions.

When the shock wave is a surface of variable curvature, the vorticity introduced by the shock wave destroys the linearity of the equations of motion. Vinokur, in his application of the method to the study of bodies of variable curvature (refs. 10 and 11), has neglected this nonlinearity in the term due to rotation. In the present work this nonlinear term is retained and a solution is found for the flow behind any axisymmetric shock with a conic longitudinal section. For bodies of bluntness zero or greater (paraboloid, sphere, or an oblate or prolate ellipsoid) numerical results for shock-wave standoff distance, body shape, and stagnation point velocity gradient are obtained and comparisons are made with the numerical calculations of Van Dyke and Gordon (ref. 4) and Mangler (ref. 5). Finally a parameter is proposed which reduces approximately any blunt body flow at a free-stream Mach number greater than 3 to an equivalent flow at infinite free-stream Mach number with a different ratio of specific heats.

The author is indebted to Dr. Max. A. Heaslet of the Ames Research Center for suggesting this problem and for his valuable advice, criticism, and encouragement during the course of the research.

LIST OF SYMBOLS

B	bluntness of conic section (see sketch (a), eq. (6))
c_p	specific heat at constant pressure
c_v	specific heat at constant volume
$\vec{e}_\varphi$	unit vector in azimuthal direction
$f_1, f_2, f_3, \ldots$	terms in series expansion of stream function (see eq. (14))
$\bar{f}_1, \bar{f}_2, \bar{f}_3, \ldots$	$\frac{1}{B} f_1 , \frac{1}{B^2} f_2 , \frac{1}{B^3} f^3$ (see eq. (19(c))
$\vec{f}(\psi)$	vorticity function, $\frac{\vec{\omega}}{r}$
h_η, h_ξ, h_φ	scale factors of the curvilinear coordinate system
$H(\psi)$	total head on the streamline ψ
k	curvature in the x, r plane
K	$\frac{\rho}{\rho_\infty}$

M	Mach number
p	pressure
r	radius in cylindrical polar coordinates measured from body axis
R_s	radius of shock wave
s	distance along body surface
$\vec{V}$	velocity
x	distance along body axis measured from shock wave
α	angle between local stream and tangent to shock wave
γ	ratio of specific heats, $\frac{c_p}{c_v}$
δ	standoff distance of shock wave from body
η	curvilinear coordinate orthogonal to ξ
$\overline{\eta}$	$\sqrt{B_s\eta^2 + 1 - B_s}$
λ	$2(K - 1)^2$
ξ	curvilinear coordinate orthogonal to η
$\overline{\xi}$	$\sqrt{1 - B_s\xi^2}$
χ	$\frac{2K}{V_\infty}\psi$
ρ	density
φ	azimuthal angle
ψ	stream function
$\vec{\omega}$	vorticity
$(\ )_B$	value associated with body
$(\ )_s$	value associated with shock
$(\ )_{st}$	value associated with stagnation point
$(\ )_\eta$	component in the η direction

$( )_\xi$	component in the ξ direction
$( )_\varphi$	component in the φ direction
$\vec{( )}$	vector quantity

FUNDAMENTAL EQUATIONS IN CURVILINEAR COORDINATES

The constant density approximation as used by Lighthill leads to an indirect method in that one begins with a known axisymmetric analytic shock wave and investigates the flow behind it. The body shape which produced the wave is then calculated. That procedure is followed here. The coordinate system is chosen so that the shock wave is a coordinate surface, $\eta = 1$; φ is the azimuthal angle; and ξ is the third member of the orthogonal coordinate system. The continuity equation for incompressible axisymmetric flow is then:

$$\operatorname{div} \vec{V} = \frac{1}{h_\varphi h_\eta h_\xi} \left[\frac{\partial}{\partial \xi} (h_\varphi h_\eta V_\xi) + \frac{\partial}{\partial \eta} (h_\varphi h_\xi V_\eta) \right] = 0 \tag{1}$$

where h_ξ, h_η, and h_φ are the local scale factors of the coordinate system.

A stream function $\psi(\xi, \eta)$ is defined in such a manner that it satisfies this equation identically.

$$\frac{\partial \psi}{\partial \eta} = h_\varphi h_\eta V_\xi \tag{2a}$$

$$\frac{\partial \psi}{\partial \xi} = -h_\varphi h_\xi V_\eta \tag{2b}$$

It is assumed that vorticity is generated only at the shock wave. It then follows that for incompressible axisymmetric flow

$$\frac{\vec{\omega}}{r} = \vec{f}(\psi) \tag{3}$$

where $\vec{\omega}$ is the vorticity, r is the distance from the axis of symmetry, and $\vec{f}(\psi)$ is some function of ψ alone. This means that if $\vec{\omega}/r$ is known at some point on a streamtube, it is known everywhere on that streamtube. Thus if $f(\psi)$ can be evaluated somewhere in the flow field, equation (3) can be used to relate (upon substitution for $\vec{\omega}$) the velocity components and hence the stream function to a known right side. Lighthill has given a result for the vorticity jump across any shock wave (at $M_\infty = \infty$) as a function of the shock curvature, density ratio, and component of velocity tangential to the shock wave. Hayes (ref. 12) has shown that

this result is independent of free-stream Mach number. Therefore $\vec{f}(\psi)$ can be regarded as a known function once the geometry of the shock is specified. When the shock wave is axisymmetric, $\vec{f}(\psi)$ has only a φ component. When the indicated substitutions are made in equation (3), the following equation results

$$\frac{\vec{e}_\varphi}{r h_\eta h_\xi}\left[-\frac{\partial}{\partial\xi}\left(\frac{h_\eta}{h_\varphi h_\xi}\frac{\partial\psi}{\partial\xi}\right)-\frac{\partial}{\partial\eta}\left(\frac{h_\xi}{h_\varphi h_\eta}\frac{\partial\psi}{\partial\eta}\right)\right]=\vec{f}(\psi) \tag{4}$$

The Equations in Van Dyke's Confocal Coordinate System

Van Dyke (ref. 3) introduced a unified axisymmetric orthogonal coordinate system that passes continuously from hyperboloidal to oblate ellipsoidal. Thus every conic coordinate system can be obtained from it as a special case. It is obtained by setting

$$\frac{x}{R_S}=\frac{1}{B_S}\left[1-\sqrt{(1-B_S\xi^2)(1-B_S+B_S\eta^2)}\right] \tag{5a}$$

$$\frac{r}{R_S}=|\xi|\eta \tag{5b}$$

where B_S is the bluntness of the shock wave. The bluntness, B, of a conic can be related to the eccentricity of that conic in the following way:

For hyperbolas and prolate ellipses:

$$B=1-e^2 \tag{6a}$$

For oblate ellipses:

$$B=\frac{1}{1-e^2} \tag{6b}$$

For both oblate and prolate ellipses, B is equal to the square of the ratio of the r axis to the x axis. A shock wave of bluntness B_S is described by $\eta = 1$.[1] The shock wave is hyperboloidal when $B_S < 0$, paraboloidal when $B_S = 0$, prolate ellipsoidal when $0 < B_S < 1$, spherical when

[1]Actually for ellipsoids, $B_S > 0$, equations (5) give only the left half of the figure. This is the only part which may form a shock.

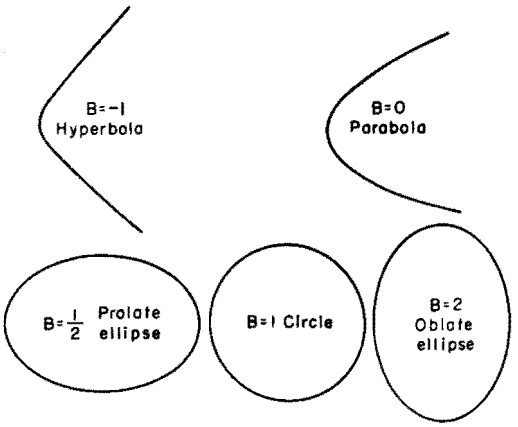

Sketch (a)

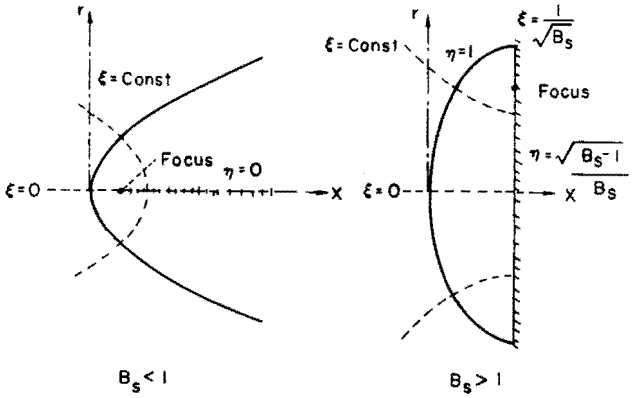

Sketch (b)

$B_S = 1$, and oblate ellipsoidal when $1 < B_S$. This is illustrated in sketch (a). The azimuthal angle is φ and the third member of the coordinate system is ξ. The coordinate system is shown in sketch (b). In the subsequent analysis, the shock-wave radius is taken to be unity. The line element is given by

$$ds^2 = \left[\frac{(1 - B_S)\xi^2 + \eta^2}{1 - B_S\xi^2}\, d\xi^2 + \frac{(1 - B_S)\xi^2 + \eta^2}{(1 - B_S) + B_S\eta^2}\, d\eta^2 + \xi^2\eta^2 d\varphi^2\right] \qquad (7)$$

Thus

$$h_\xi = \sqrt{\frac{(1 - B_S)\xi^2 + \eta^2}{1 - B_S\xi^2}} \tag{8a}$$

$$h_\eta = \sqrt{\frac{(1 - B_S)\xi^2 + \eta^2}{1 - B_S + B_S\eta^2}} \tag{8b}$$

$$h_\varphi = \xi\eta \tag{8c}$$

The function $\vec{f}(\psi)$ will now be evaluated. For an axisymmetric shock wave in a uniform flow, Lighthill's result for the vorticity after the shock is

$$\vec{\omega} = \vec{e}_\varphi \frac{(K - 1)^2}{K} V_t k \tag{9}$$

where V_t is the component of free-stream velocity tangential to the shock wave in the x, r plane; k is the curvature of the shock wave in the x, r plane; and K is ρ/ρ_∞. Using the definition of curvature, the fact that the shock wave is given by equations (5) with η set equal to unity, and equation (9) we obtain

$$\vec{f}(\psi) = -\vec{e}_\varphi \frac{(K - 1)^2}{K} \frac{V_\infty}{[1 + (1 - B_S)r^2]^2} \tag{10}$$

At the shock wave

$$\psi = \frac{V_\infty}{2K} r^2$$

Therefore at the shock wave

$$\vec{f}(\psi) = -\vec{e}_\varphi \frac{(K - 1)^2}{K} \frac{V_\infty}{\left[1 + (1 - B_S)\frac{2K}{V_\infty}\psi\right]^2} \tag{11}$$

However, since $\vec{f}(\psi)$ must remain fixed on streamlines, this expression is applicable to the entire flow field after the shock. Equation (4) then becomes, on substitution of equations (8) and (11):

$$\frac{\partial}{\partial\xi}\left[\frac{1}{\xi\eta}\left(\frac{1 - B_S\xi^2}{1 - B_S + B_S\eta^2}\right)^{1/2}\frac{\partial\chi}{\partial\xi}\right] + \frac{\partial}{\partial\eta}\left[\frac{1}{\xi\eta}\left(\frac{1 - B_S + B_S\eta^2}{1 - B_S\xi^2}\right)^{1/2}\frac{\partial\chi}{\partial\eta}\right]$$

$$= \frac{\lambda\xi\eta[(1 - B_S)\xi^2 + \eta^2]}{[(1 - B_S\xi^2)(1 - B_S + B_S\eta^2)]^{1/2}[1 + (1 - B_S)\chi]^2} \tag{12}$$

where

$$\chi = \frac{2K}{V_\infty}\psi$$

$$\lambda = 2(K - 1)^2$$

The boundary conditions, which express the continuity of mass and the tangential component of velocity across the shock, are:

$$\chi(\xi, 1) = \xi^2 \tag{13a}$$

$$\frac{\partial \chi}{\partial \eta}(\xi, 1) = 2K\xi^2 \tag{13b}$$

A solution of equation (12) satisfying the boundary conditions (eqs. (13)) would give the details of the flow behind any shock wave of conic longitudinal section (subject, of course, to the inexactness of the constant density approximation). This equation is, however, nonlinear because of its right side and an exact solution to it would be very difficult to obtain. It is reasonable to seek a series solution near the stagnation point because here the constant density approximation is most faithful.

Series Solution near the Stagnation Point

To obtain a series solution we set

$$\chi = \sum_{n=1}^{\infty} \xi^{2n} f_n(\eta) \tag{14}$$

where the odd powers of ξ in the expansion can be suppressed by virtue of the geometric symmetry about the x axis. This expression is then substituted into equation (12) and coefficients of like powers of ξ are set equal to zero. The following infinite set of ordinary differential equations is then obtained:

$$(1 - B_s + B_s\eta^2)\frac{d}{d\eta}\left(\frac{1}{\eta}\frac{df_1}{d\eta}\right) + B_s\frac{df_1}{d\eta} + \frac{1}{\eta}(8f_2 - 2B_sf_1) = \lambda\eta^3 \tag{15a}$$

$$(1 - B_s + B_s\eta^2)\frac{d}{d\eta}\left(\frac{1}{\eta}\frac{df_2}{d\eta}\right) + B_s\frac{df_2}{d\eta} + \frac{1}{\eta}(24f_3 - 12B_sf_2)$$

$$= \lambda(1 - B_s)(\eta - 2\eta^3 f_1) \tag{15b}$$

$$(1 - B_S + B_S\eta^2)\frac{d}{d\eta}\left(\frac{1}{\eta}\frac{df_3}{d\eta}\right) + B_S\frac{df_3}{d\eta} + \frac{1}{\eta}(48f_4 - 30B_Sf_3)$$

$$= \lambda(1 - B_S)[3(1 - B_S)\eta^3f_1^2 - 2(1 - B_S)\eta f_1 - 2\eta^3f_2] \qquad (15c)$$

etc. On substitution of (14) into equations (13) the boundary conditions become:

$$f_1(1) = 1 \qquad (16a)$$

$$\frac{df_1}{d\eta}(1) = 2K \qquad (16b)$$

$$f_i(1) = \frac{df_i}{d\eta}(1) = 0 \quad , \qquad i > 1 \qquad (16c)$$

A coupling between this set of ordinary differential equations is seen to exist, except for $B_S = 1$. In this latter case the right sides of all the above equations except the first become zero and this in conjunction with the boundary conditions implies that[2]

$$f_i \equiv 0 \quad , \qquad i > 1$$

When $B_S \neq 1$ it would seem, however, that a knowledge of f_2 is necessary to calculate f_1, etc. A power series expansion about $\eta = 1$ is, however, possible. Since $f_2(1)$ and $df_2/d\eta(1)$ are both known from the boundary conditions (are in fact zero), $d^2f_1/d\eta^2(1)$ and $d^3f_1/d\eta^3(1)$ can both be evaluated from the first equation, and $d^2f_2/d\eta^2(1)$ and $d^3f_2/d\eta^3(1)$ can then be evaluated from the second equation. This process can be carried on indefinitely. The following series expansion for χ is then obtained.

$$\chi = \xi^2f_1(\eta) + \xi^4f_2(\eta) + \xi^6f_3(\eta) + \xi^8f_4(\eta) + \xi^{10}f_5(\eta) + \cdots \qquad (17)$$

where

---

[2]Vinokur's assumption that the nonlinearity in the term due to rotation is unimportant also leads to this result and he therefore needs to integrate only equation (15a).

$$f_1(\eta) = 1 - 2K(1-\eta) + [-(K-1)B_s + (K^2 - K + 1)](1-\eta)^2 + \Big[-(K-1)B_s^2 + \frac{1}{3}(K-1)(3K-2)B_s - \frac{5}{3}(K-1)^2\Big](1-\eta)^3 + \frac{1}{4}(K-1)\Big[-5B_s^3 + (5K-3)B_s^2 - \frac{1}{3}(34K-35)B_s + \frac{23}{3}(K-1)\Big](1-\eta)^4 + \frac{1}{2}(K-1)\Big[-\frac{7}{2}B_s^4 + \frac{1}{2}(7K+3)B_s^3 - \frac{1}{30}(280K-283)B_s^2 + \frac{1}{30}(32K^2 + 245K - 275)B_s - \frac{1}{15}(K-1)(16K+47)\Big](1-\eta)^5 + (K-1)\Big[-\frac{21}{2}B_s^5 + \frac{7}{6}(9K-2)B_s^4 - \frac{1}{6}(189K-186)B_s^3 + \frac{1}{30}(160K^2 + 987K - 1144)B_s^2 + \frac{1}{90}(-32K^3 - 736K^2 - 1236K + 2011)B_s + \frac{1}{45}(K-1)(16K^2 + 144K + 251)\Big](1-\eta)^6 + \cdots \qquad (18a)$$

$$f_2(\eta) = (K-1)^2\Big\{(B_s-1)(1-\eta)^2 + \Big[B_s^2 - \frac{2}{3}(2K+5)B_s + \frac{1}{3}(4K+7)\Big](1-\eta)^3 + \frac{1}{12}[15B_s^3 - (24K+61)B_s^2 + (4K^2 + 56K + 101)B_s - (4K^2 + 32K + 55)](1-\eta)^4 + \frac{1}{60}[105B_s^4 - 5(36K+95)B_s^3 + (40K^2 + 612K + 983)B_s^2 - (112K^2 + 700K + 985)B_s + 4(18K^2 + 67K + 93)](1-\eta)^5\Big\} + \cdots \qquad (18b)$$

$$f_3(\eta) = (K-1)^2\Big\{(B_s-1)^2(1-\eta)^2 + \frac{1}{3}[3B_s^2 - (8K+15)B_s^2 + (16K+21)B_s - (8K+9)](1-\eta)^3 + \frac{1}{12}[15B_s^4 - 8(6K+11)B_s^3 + 2(18K^2 + 84K + 115)B_s^2 - 4(18K^2 + 48K + 64)B_s + 9(4K^2 + 8K + 11)](1-\eta)^4\Big\} + \cdots \qquad (18c)$$

$$f_4(\eta) = (K-1)^2\left\{(B_s-1)^3(1-\eta)^2 + \frac{1}{3}\left[3B_s^4 - 4(3K+5)B_s^3 + 6(6K+7)B_s^2 - 36(K+1)B_s + (12K+11)\right](1-\eta)^3\right\} + \cdots \quad (18d)$$

$$f_5(\eta) = (K-1)^2(B_s-1)^4(1-\eta^2) + \cdots \quad (18e)$$

The question of convergence of the double series now arises. Since no general expression was found for the terms in the series, it was not possible to investigate the convergence directly. It can be verified by direct substitution, however, that for $|B_s| < 1$, the terms decrease sufficiently rapidly that the series appears to be of practical value for computation. For $|B_s| > 1$ the terms decrease so slowly that the series is of little value. A transformed version of this series will therefore be given which does converge sufficiently rapidly for all positive B_s.

Transformation of the Series

The transformations

$$\bar{\xi} = \sqrt{1 - B_s\xi^2} \quad (19a)$$

$$\bar{\eta} = \sqrt{B_s\eta^2 + 1 - B_s} \quad (19b)$$

$$\bar{f}_n = \frac{1}{B_s{}^n} f_n \quad (19c)$$

when applied to equations (15) give the following result:

$$\frac{d^2\bar{f}_1}{d\bar{\eta}^2} + (8\bar{f}_2 - 2\bar{f}_1)\frac{1}{\bar{\eta}^2 - 1 + B_s} = \frac{\lambda}{B_s{}^4}(\bar{\eta}^2 - 1 + B_s) \quad (20a)$$

$$\frac{d^2\bar{f}_2}{d\bar{\eta}^2} + (24\bar{f}_3 - 12\bar{f}_2)\frac{1}{\bar{\eta}^2 - 1 + B_s} = \frac{\lambda}{B_s{}^4}\left[1 - B_s - 2(1-B_s)(\bar{\eta}^2 - 1 + B_s)\bar{f}_1\right] \quad (20b)$$

$$\frac{d^2\bar{f}_3}{d\bar{\eta}^2} + (48\bar{f}_4 - 30\bar{f}_3)\frac{1}{\bar{\eta}^2 - 1 + B_s} = \frac{\lambda}{B_s{}^4}\left[-2(1-B_s)\bar{f}_1 - 2(1-B_s)(\bar{\eta}^2 - 1 + B_s)\bar{f}_2 + 3(1-B_s)^2(\bar{\eta}^2 - 1 + B_s)\bar{f}_1{}^2\right] \quad (20c)$$

The boundary conditions become, using (19) and (16)

$$\bar{f}_1(1) = \frac{1}{B_S} \tag{21a}$$

$$\frac{d\bar{f}_1}{d\bar{\eta}}(1) = \frac{2K}{B_S^2} \tag{21b}$$

$$\bar{f}_i(1) = \frac{d\bar{f}_i}{d\bar{\eta}}(1) = 0 \quad , \qquad i > 1 \tag{21c}$$

The following double series for χ can now be obtained either by transformation of equations (17) and (18) or by straightforward solution of equations (20) in the manner previously indicated.

$$\chi = (1 - \bar{\xi}^2)\bar{f}_1(\bar{\eta}) + (1 - \bar{\xi}^2)^2\bar{f}_2(\bar{\eta}) + (1 - \bar{\xi}^2)^3\bar{f}_3(\bar{\eta})(1 - \bar{\xi}^2)^4\bar{f}_4(\bar{\eta}) + (1 - \bar{\xi}^2)^5\bar{f}_5(\bar{\eta}) + \cdots \tag{22}$$

where

$$\begin{aligned}\bar{f}_1(\bar{\eta}) = {} & B_S^{-1} - 2K(1 - \bar{\eta})B_S^{-2} + B_S^{-2}[1 + (K - 1)^2B_S^{-1}](1 - \bar{\eta})^2 \\ & - \frac{2}{3}(K - 1)B_S^{-3}[1 + (K - 1)B_S^{-1}](1 - \bar{\eta})^3 \\ & - \frac{1}{3}(K - 1)B_S^{-4}[(K + 1) - 2(K - 1)B_S^{-1}](1 - \bar{\eta})^4 \\ & + \frac{2}{15}(K - 1)B_S^{-4}[1 + 4K^2 - 5K - 5)B_S^{-1} \\ & - 2(K - 1)(2K - 1)B_S^{-1}](1 - \bar{\eta})^5 + \frac{2}{45}(K - 1)B_S^{-5}[3(2K + 1) \\ & - (2K^3 - 14K^2 + 37K - 1)B_S^{-1} + 2(K - 1)(K^2 - 6K + 11)B_S^{-2}](1 - \bar{\eta})^6 \\ & + \cdots\end{aligned} \tag{23a}$$

$$\begin{aligned}\bar{f}_2(\bar{\eta}) = (K - 1)^2\Big\{ & (B_S - 1)B_S^{-4}(1 - \bar{\eta})^2 - \frac{4}{3}B_S^{-4}[(1 - B_S^{-1})(K + 1)](1 - \bar{\eta})^3 \\ & - \frac{1}{3}B_S^{-4}[1 - (K^2 + 2K + 8) + (K^2 + 2K + 7)B_S^{-2}](1 - \bar{\eta})^4 \\ & + \frac{2}{15}B_S^{-5}[(14K + 1) - (4K^2 + 30K + 5)B_S^{-1} \\ & + (4K^2 + 6K + 4)B_S^{-2}](1 - \bar{\eta})^5\Big\} + \cdots\end{aligned} \tag{23b}$$

$$\bar{f}_3(\bar{\eta}) = (K-1)^2\left\{(1-B_S^{-1})B_S^{-3}(1-\bar{\eta})^2 - \frac{2}{3}(1-B_S^{-1})B_S^{-4}(4K+3)(1-\bar{\eta})^3\right.$$

$$-\frac{1}{3}B_S^{-4}[1-(9K^2+6K+15)-(9K^2+6K+17)B_S^{-1}$$

$$\left.+(18K^2+12K+31)B_S^{-2}](1-\bar{\eta})^4\right\}+\cdots \tag{23c}$$

$$\bar{f}_4(\bar{\eta}) = (K-1)^2\left[(1-B_S^{-1})B_S^{-3}(1-\bar{\eta})^2\right.$$

$$\left.-\frac{4}{3}(1-B_S^{-1})B_S^{-4}(3K+2)(1-\bar{\eta})^3\right]+\cdots \tag{23d}$$

$$\bar{f}_5(\bar{\eta}) = (K-1)^2\left[(1-B_S^{-1})^4B_S^{-3}(1-\bar{\eta})^2\right]+\cdots \tag{23e}$$

The following computation was undertaken to obtain information about the convergence of the series in equation (22). The first of equations (20) was integrated numerically assuming $\bar{f}_2 = 0$. The first two equations were then integrated simultaneously assuming $\bar{f}_3 = 0$. This process was continued through the simultaneous integration of the first five equations. The results were then compared with each other and with numerical values given by the series. A typical result is shown in table I.

It can be seen from table I that $\bar{f}_1$ is only slightly affected by the addition of the other $\bar{f}$'s. It is, therefore, reasonable to suppose that the results from the simultaneous integration of the first five of equations (20) are for all practical purposes the exact solution for $\bar{f}_1$. The series solution is then seen to be extremely close to the exact solution.

CALCULATION OF FLOW QUANTITIES

Standoff Distance and Body Bluntness

The stream function has been so chosen that the axis of symmetry is the zero streamline. When this streamline reaches the body it wets the entire surface. The body can then be located by examining the zeros of the stream function. Near the axis, $\bar{\xi} = 1$,

$$\chi \approx \bar{f}_1(\bar{\eta})$$

The body shape near the axis is therefore given by a zero of $\bar{f}_1$, and since $\bar{f}_1$ is a function of $\bar{\eta}$ alone, the body is necessarily a confocal ellipse.

Away from the stagnation point, $1 - \bar{\xi}^2$ is not very much less than 1, and the body surface is not given by a zero of $\bar{f}_1$. The body coordinates are solutions of the equation:

$$\bar{f}_1(\bar{\eta}) + (1 - \bar{\xi}^2)\bar{f}_2(\bar{\eta}) + \cdots = 0$$

The magnitudes of $\bar{f}_2$, $\bar{f}_3$, . . . have been investigated both from the series obtained and by numerical integration of the differential equations. It was found that these functions are sufficiently small that, in the region where the initial assumptions can be expected to hold, they are negligible. The body is considered, therefore, to be a conic. Following references 3 and 5 bodies obtained here are characterized by a bluntness B_B. The bluntness of an ellipse defined by $\bar{\eta} = \bar{\eta}_B$ is (from eqs. (5), (6), and (19b))

$$B_B = \frac{\bar{\eta}_B^2 - 1 + B_S}{\bar{\eta}_B^2} \tag{24}$$

This quantity together with the body nose radius completely specified the body shape. The body radius R_B when referred to the shock-wave radius can be expressed as (from eqs. (5) and (19b) and the definition of radius of curvature)

$$\frac{R_B}{R_S} = \frac{\bar{\eta}_B^2 - 1 + B_S}{B_S \bar{\eta}_B} \tag{25}$$

For very large K, an approximate zero of $\bar{f}_1$ can be found (from eq. (23a)). When this value of $\bar{\eta}$ is substituted in equation (5a) and in equation (24), the following relations result:

$$\frac{\delta}{R_B} = \frac{1}{K} - \sqrt{\frac{8}{3}}\frac{1}{K^{3/2}} + \frac{5 - B_B}{K^2} + \cdots \tag{26}$$

$$\frac{R_B}{R_S} = 1 + \frac{B_B - 2}{K} - \sqrt{\frac{8}{3}}\frac{B_B - 2}{K^{3/2}} + \cdots \tag{27}$$

Equation (26) is in agreement with the result given by Hayes[3] (ref. 9) for $B_B = 1$.

If the shock-wave shape is held constant and K varied, the body shape will, in general, change. Figures which show standoff distance and shock radius for a given body as a function of K are, therefore, cross

---

[3]Since Hayes presents δ/R_s, equation (27) must be used to show that (26) is identical to Hayes' result for $B_B = 1$.

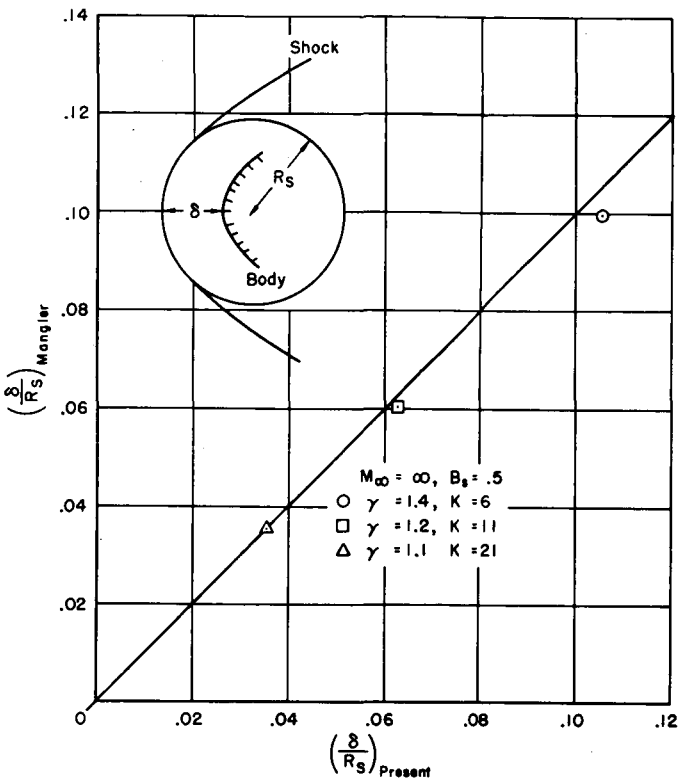

Sketch (c)

plots. Sketch (c) compares standoff distance calculated by the present theory to that given in reference 5 for a shock of bluntness one half. At $K = 6(\gamma = 1.4)$, the present calculation differs from reference 5 by 5.8 percent, whereas at $K = 21(\gamma = 1.1)$, the difference is only 0.3 percent. Thus it seems that for small γ the constant density approximation is very accurate. Figure 1 gives the ratio of standoff distance to body nose radius as a function of K for a large number of bodies. Vinokur's results are shown for comparison.

Figure 2 compares body radius obtained from the constant density approximation to results of reference 4. It can be seen that the constant density approximation predicts a larger body radius than does the exact computation.

Figure 3 gives body bluntness as a function of shock-wave bluntness for several γ. Further blunt-body solutions of the type presented in reference 4 have been obtained at the Ames Research Center by Mr. Franklyn B. Fuller and two of these results are plotted for comparison. It can be seen that the exact computation predicts a larger body bluntness than does the constant density approximation. This disagreement decreases for smaller γ, and for $\gamma = 1$ both methods give the same result.

Stagnation Point Velocity Gradient

The gradient of the velocity at the stagnation point is

$$\frac{R_S}{V_\infty}\left(\frac{dV}{ds}\right)_{st} = \frac{B_S{}^3\bar{f}_1{}'(\bar{\eta})}{2K(\bar{\eta}^2 + B_S - 1)} \tag{28}$$

In the table below, stagnation point velocity gradient is compared with that of reference 5. As can be seen, the agreement is better for small γ. It is also evident that the constant density approximation gives a reasonably accurate estimate of the stagnation point velocity gradient even for $\gamma = 1.4$.

M_∞	γ	B_S	$\frac{R_S}{V_\infty}\left(\frac{dV}{ds}\right)_{st}$		Percent error
			Ref. 8	Present	
∞	1.4	1/2	0.7645	0.7564	1.06
∞	1.2	1/2	0.5332	0.5296	0.68
∞	1.1	1/2	0.3723	0.3712	0.30

For large K the following result can be derived for stagnation point velocity gradient

$$\frac{R_B}{V_\infty}\left(\frac{dV}{ds}\right)_{st} = \sqrt{\frac{8}{3}}\,\frac{1}{K^{1/2}} + \frac{26B - 269}{9\sqrt{8/3}\,K^{3/2}} + \cdots \tag{29}$$

Hayes gives the first term of equation (29) in reference 9. The functional form of equation (29) is in agreement with the expansion for large K of the classical result given by Li and Geiger (ref. 13) with the constants differing slightly. Neither of these latter results includes the effect of body bluntness.

Figure 4 is a plot of stagnation-point velocity gradient as a function of body bluntness and K. Vinokur's results are shown for comparison.

Pressure Distribution on the Body

The vector momentum equation for incompressible flow can be written

$$\vec{V} \times \text{Curl } \vec{V} = \text{grad}\left(\frac{p}{\rho} + \frac{V^2}{2}\right) \tag{30}$$

Scalar multiplication of equation (30) by $\vec{V}$ yields

$$\vec{V}\cdot\nabla\left(\frac{p}{\rho}+\frac{V^2}{2}\right)=0 \tag{31}$$

where $\vec{V}\cdot\nabla$ is a derivative in the direction $\vec{V}$ and is therefore the derivative along a streamline. The above equation expresses the fact that

$$\frac{p}{\rho}+\frac{V^2}{2}=H(\psi) \tag{32}$$

Equation (32) is the Bernoulli equation for incompressible rotational flow. The pressure variation on any streamline in the flow can be calculated from it (presuming that H is known at some point on the streamline). It is evident from symmetry that the streamline which passes through the normal shock wets the body surface. Using the strong shock relations to evaluate the pressure, density, and velocity behind the normal shock one obtains

$$H(0)=\frac{V_\infty^2}{K}\left(\frac{1}{2K}+\frac{2\gamma}{\gamma+1}\right) \tag{33}$$

The pressure on the body surface is then

$$\frac{p}{(1/2)\rho_\infty V_\infty^2}=\frac{1}{K}+\frac{4\gamma}{\gamma+1}-K\left(\frac{V}{V_\infty}\right)^2 \tag{34}$$

and $(V/V_\infty)^2$ is then computed from the stream function. Taking account of the facts that on the body surface $f_1(\psi)$ is nearly zero, and that near the axis $(1-\bar{\xi}^2)\ll 1$ this equation becomes

$$\frac{p}{(1/2)\rho_\infty V_\infty^2}\approx\frac{1}{K}+\frac{4\gamma}{\gamma+1}+\frac{B_s^4}{4K^2}\,\frac{1-\bar{\xi}^2}{\bar{\eta}^2+(B_s-1)\bar{\xi}^2}\,[\bar{f}_1'(\bar{\eta})]^2 \tag{35}$$

Figure 5 is a plot of the pressure distributions on a sphere given by the constant density approximation and by Van Dyke and Gordon (ref. 4).

APPLICATION TO FLOW AT FINITE FREE-STREAM MACH NUMBER

In the preceding analysis it was convenient to assume that the free-stream Mach number was infinite because of the fact that as a consequence of the shock-wave relations, the density is constant just after the shock wave only if the Mach number is infinite. It will be shown, however, that near the axis of symmetry, the variation in density is not great at moderately high free-stream Mach numbers.

The density ratio across a shock wave satisfies the equation

$$\frac{\rho}{\rho_\infty} = \frac{\gamma + 1}{\gamma - 1 + (2/M_\infty^2 \sin^2\alpha)} \tag{36}$$

where α is the angle of inclination of the shock wave to the free stream. It can be seen from this equation that if attention is restricted to a small region containing the normal portion of the shock wave ($\alpha \approx \pi/2$), the variation in ρ/ρ_∞ can be made as small as desired. Then $\sin\alpha$ is approximately 1 and we have the following relation for K:

$$K = \frac{\gamma + 1}{\gamma - 1 + (2/M_\infty^2)} \tag{37}$$

It can be concluded from the preceding argument and from the fact that Hayes has shown that Lighthill's result for the vorticity after a shock holds at finite free-stream Mach number, that the results arrived at previously can reasonably be applied to a small region of the flow behind a shock wave in a flow with finite free-stream Mach number. The flow downstream of the shock wave is seen then to be a function of B_S and K or, for a given shock wave, K alone. This means that (within the limits of applicability of this theory) a flow at any γ and free-stream Mach number has an analog at $M_\infty = \infty$ and a different γ. Fuller's numerical solutions have been used to test the validity of this parameter. Figure 6 shows the result of two calculations, one at $M_\infty = 3$, $\gamma = 1.4$ and the other at $M_\infty = \infty$ and $\gamma = 1.7$. In both cases

$$B_S = 0.25$$

$$\frac{\gamma + 1}{\gamma - 1 + (2/M_\infty^2)} = 3.857$$

It can be seen that the two bodies are very similar in shape, and that the shock-wave standoff distances are nearly the same. The pressure distributions are almost identical. Figure 7 shows standoff distance for finite free-stream Mach number and shock bluntness of one-half plotted against $(\gamma + 1)/(\gamma - 1)$ in one case and $\{(\gamma + 1)/[\gamma - 1 + (2/M_\infty^2)]\}$ in the other. The exact solutions are from references 4 and 5 and Fuller.

In both cases (i.e., body shape and standoff distance) the correlation is better at higher free-stream Mach number.

CONCLUDING REMARKS

A solution has been presented for the flow after axisymmetric shock waves with conic longitudinal sections. The flow behind the shock wave

has been assumed incompressible but vortical, and the nonlinearity in the term due to rotation has been retained. Shock-wave standoff distance, body bluntness, and stagnation point velocity gradient have been presented for bodies of bluntness greater than zero. Pressure distribution on a sphere has been presented also. Stagnation point velocity gradient is in very good agreement with that presented in reference 5. The agreement of standoff distance with results of references 4 and 5 is reasonably good (5.8 percent) at $\gamma = 1.4$ and improves with decreasing γ (0.3 percent at $\gamma = 1.1$). Thus it can be concluded that at high supersonic Mach numbers and for γ near one, compressibility is unimportant, but vorticity is important.

The quantities mentioned above, standoff distance, stagnation point velocity gradient, and body bluntness, agree with those presented by Vinokur. It therefore appears that he was justified in neglecting the nonlinear part of the term due to rotation.

A parameter has been proposed which approximately correlates the flow after geometrically similar shock waves at different free-stream Mach numbers. It is hoped that this parameter may prove useful in cataloging numerical blunt-body solutions.

Ames Research Center
National Aeronautics and Space Administration
Moffett Field, Calif., Feb. 27, 1961.

REFERENCES

1. Belotserkovsky, O. M.: Flow Past a Symmetrical Profile with a Detached Shock Wave. Prikl. Mat. i Mekh., vol. 22, no. 2, Mar.-Apr. 1958, pp. 206-219. (Russian)

2. Garabedian, P. R., and Lieberstein, H. M.: On the Numerical Calculation of Detached Bow Shock Waves in Hypersonic Flow. Jour. Aero. Sci., vol. 25, no. 2, Feb. 1958, pp. 109-118.

3. Van Dyke, Milton D.: The Supersonic Blunt-Body Problem - Review and Extension. Jour. Aero. Sci., vol. 25, no. 8, Aug. 1958. pp. 485-496.

4. Van Dyke, Milton D., and Gordon, Helen D.: Supersonic Flow Past a Family of Blunt Axisymmetric Bodies. NASA Rep. R-1, 1959.

5. Mangler, K. W.: The Calculation of the Flow Field Between a Blunt Body and the Bow Wave. Hypersonic Flow, Butterworths Scientific Publications, 1960, pp. 219-237. (Proc. Eleventh Symposium of the Colston Research Society, Univ. of Bristol, April 6-8, 1959.)

6. Lighthill, M. J.: Dynamics of a Dissociating Gas. Part I: Equilibrium Flow. Jour. Fluid Mech., vol. 2, pt. 1, Jan. 1957, pp. 1-32.

7. Hida, Kinzo: An Approximate Study on the Detached Shock Wave in Front of a Circular Cylinder and a Sphere. Jour. Phys. Soc. of Japan, vol. 8, no. 6, Nov.-Dec. 1953, pp. 740-745. (Also vol. 10, no. 1, Jan. 1955, pp. 79-81.)

8. Whitham, G. B.: A Note on the Stand-Off Distance of the Shock in High Speed Flow Past a Circular Cylinder. Comm. on Pure and Applied Math., vol. 10, no. 4, Nov. 1957, pp. 531-535.

9. Hayes, W. D.: Constant-Density Solutions. Ch. 4 of Hypersonic Flow Theory by Hayes, Wallace D., and Probstein, Ronald F. Academic Press, 1959, pp. 139-165.

10. Vinokur, Marcel: Inviscid Hypersonic Flow Near the Stagnation Point of Oblate Ellipsoidal Noses. Jour. Aero. Sci., vol. 25, no. 7, July 1958, pp. 469-470.

11. Vinokur, M.: Inviscid Hypersonic Flow Around Blunt Bodies. Lockheed Missiles and Space Division, LMSD-48381, General Research in Flight Sciences, Vol. II, Fluid Mechanics: Inviscid Flows, Jan. 1959, pp. 1-39.

12. Hayes, Wallace D.: The Vorticity Jump Across a Gasdynamic Discontinuity. Jour. Fluid Mech., vol. 2, pt. 6, Aug. 1957, pp. 595-600.

12. Li, Ting-Yi, and Geiger, Richard E.: Stagnation Point of a Blunt Body in Hypersonic Flow. Jour. Aero. Sci., vol. 24, no. 1, Jan. 1957, pp. 25-32.

TABLE I.- COMPARISON OF RESULTS OF NUMERICAL INTEGRATION WITH THOSE OBTAINED FROM POWER SERIES

$\bar{\eta}$	$\bar{f}_1(\bar{\eta})$ for $B_s = 10.0$, $K = 11$					
	Numerical integration with $\bar{f}_i = 0$					Series
	$i > 1$	$i > 2$	$i > 3$	$i > 4$	$i > 5$	
1.0	0.10000	0.10000	0.10000	0.10000	0.10000	0.10000
.9	.07909	.07909	.07909	.07909	.07909	.07909
.8	.06030	.06030	.06030	.06030	.06030	.06030
.7	.04356	.04353	.04353	.04353	.04353	.04353
.6	.02882	.02871	.02871	.02871	.02871	.02871
.5	.01601	.01578	.01578	.01578	.01578	.01578
.4	.00508	.00467	.00467	.00467	.00467	.00468
.35208 $= \bar{\eta}_B$	$< 10^{-3}$	$< 10^{-4}$	$< 10^{-4}$	$< 10^{-4}$	$< 10^{-4}$	0

Page intentionally left blank

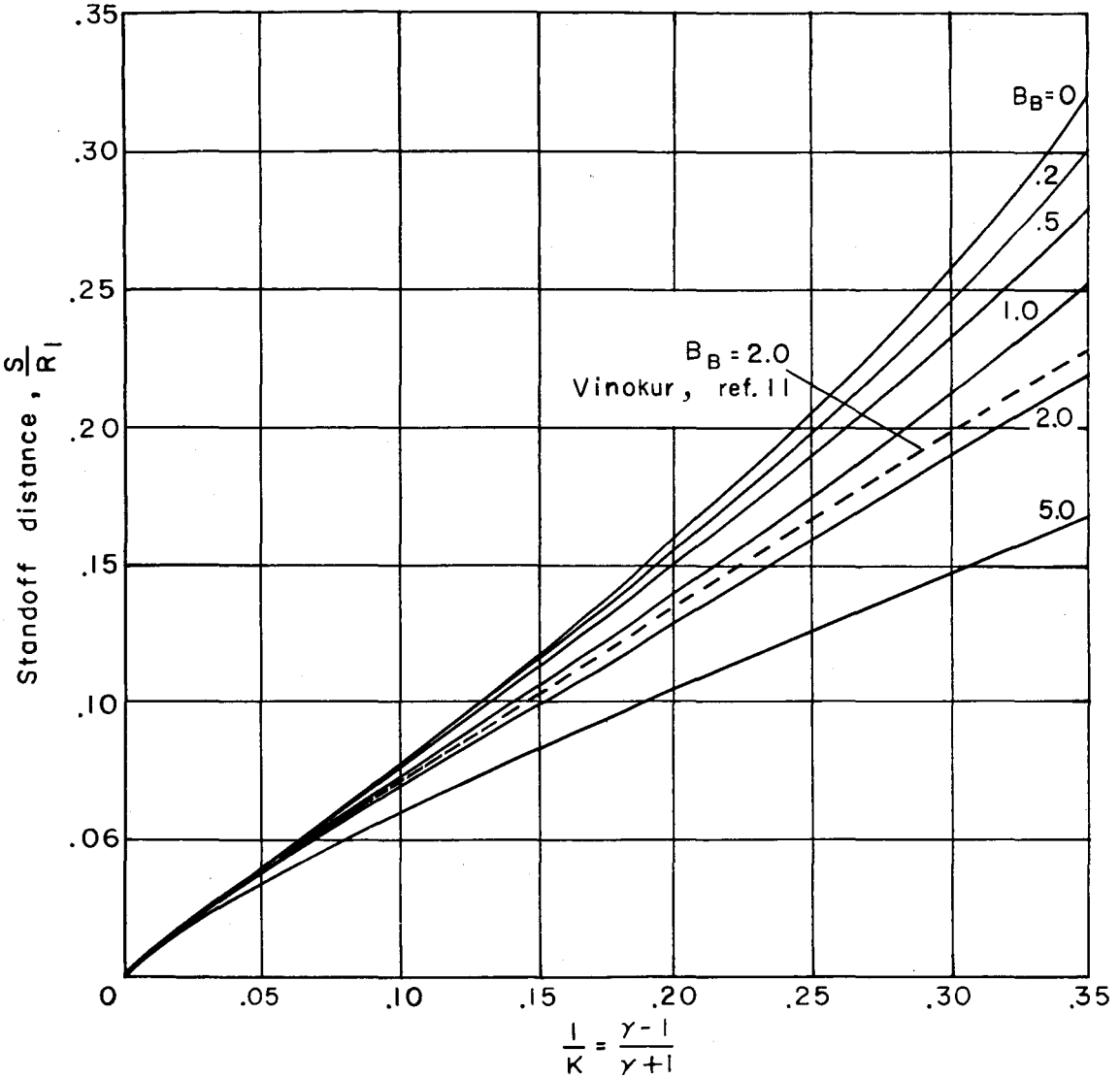

Figure 1.- Shock wave standoff distance for various values of bluntness parameter, B_B.

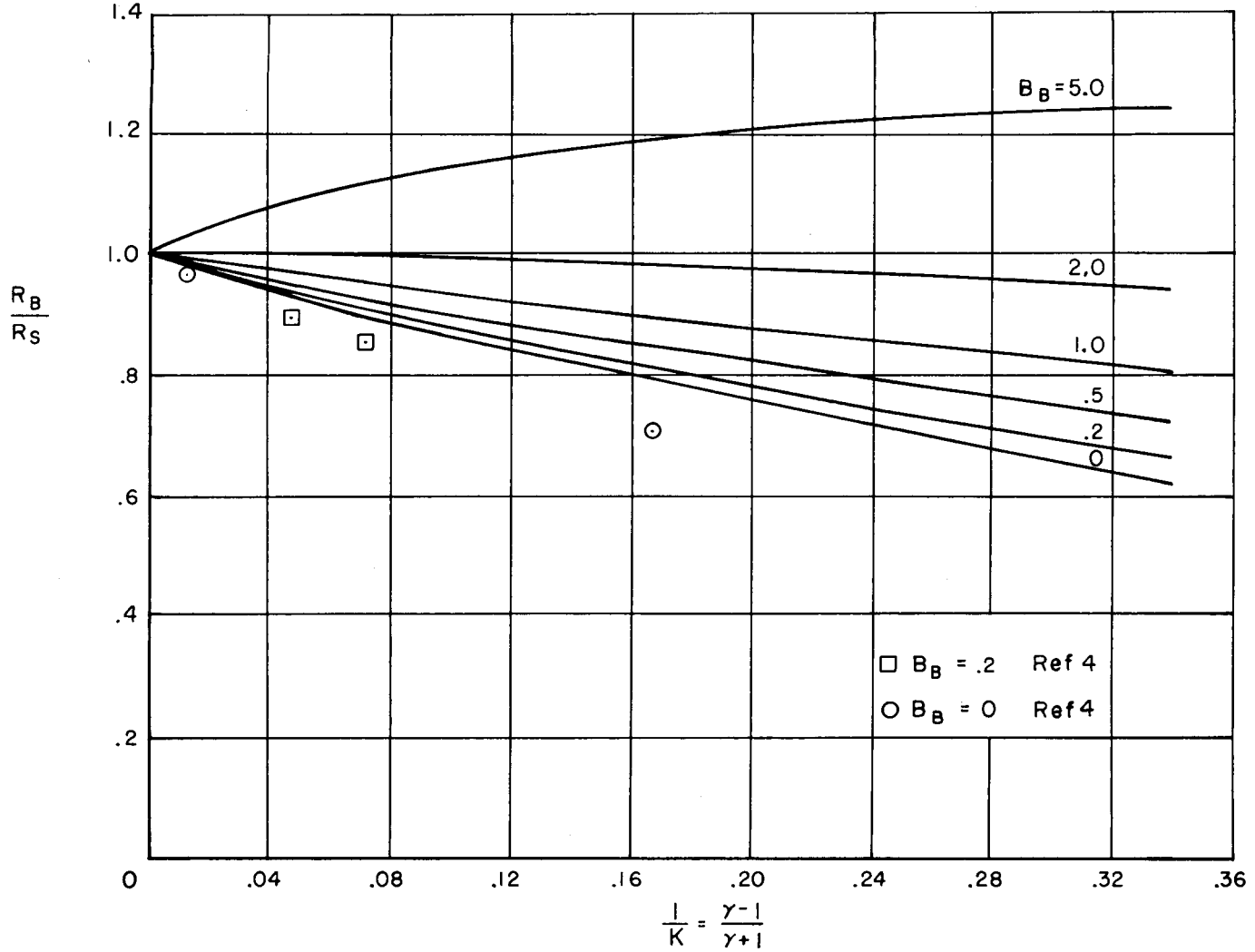

Figure 2.- Body nose radius of curvature at $M_\infty = \infty$ for several values of bluntness parameter, B_B.

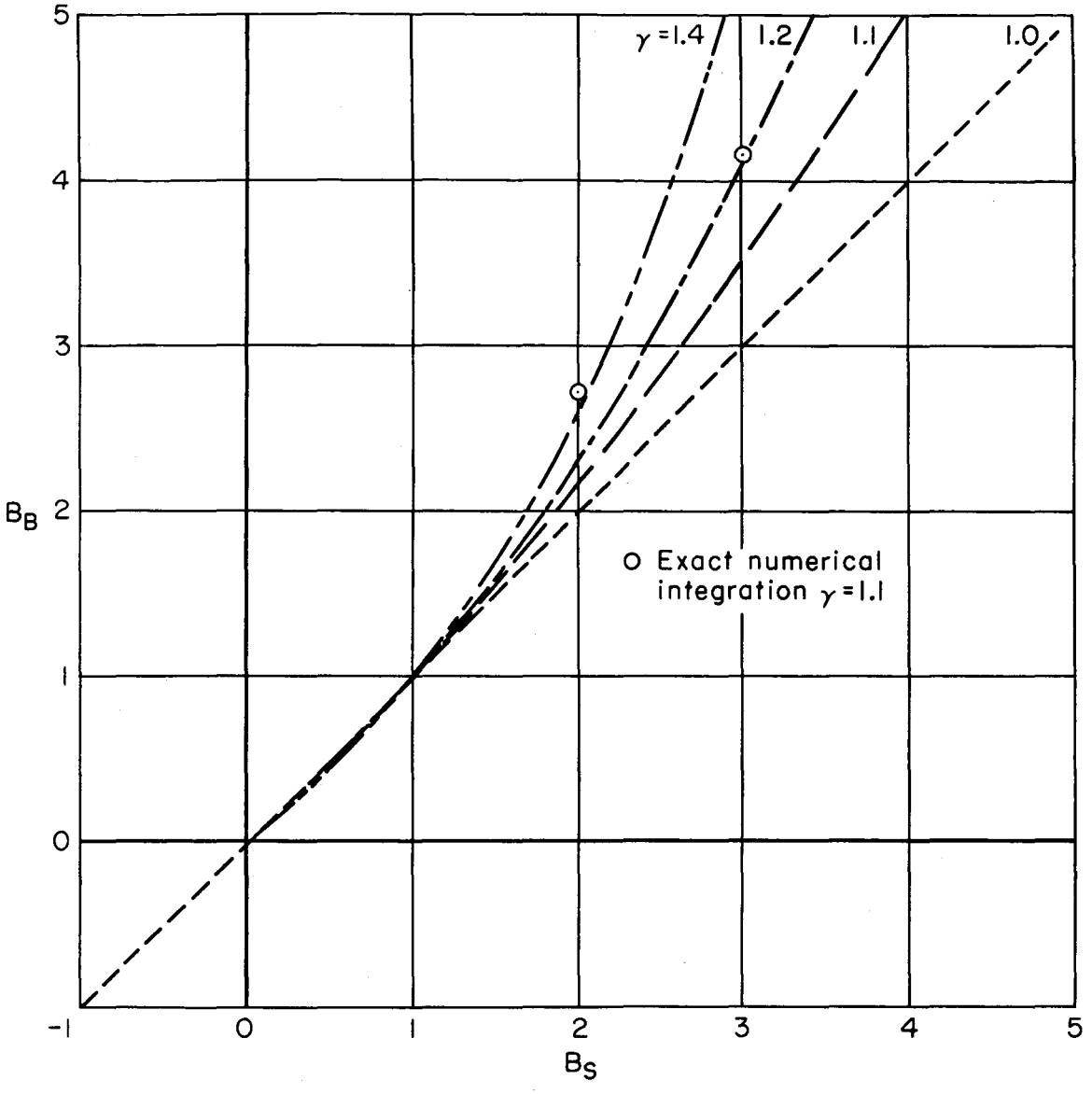

Figure 3.- Variation of body bluntness with shock wave bluntness for $M_\infty = \infty$; comparison with numerical results.

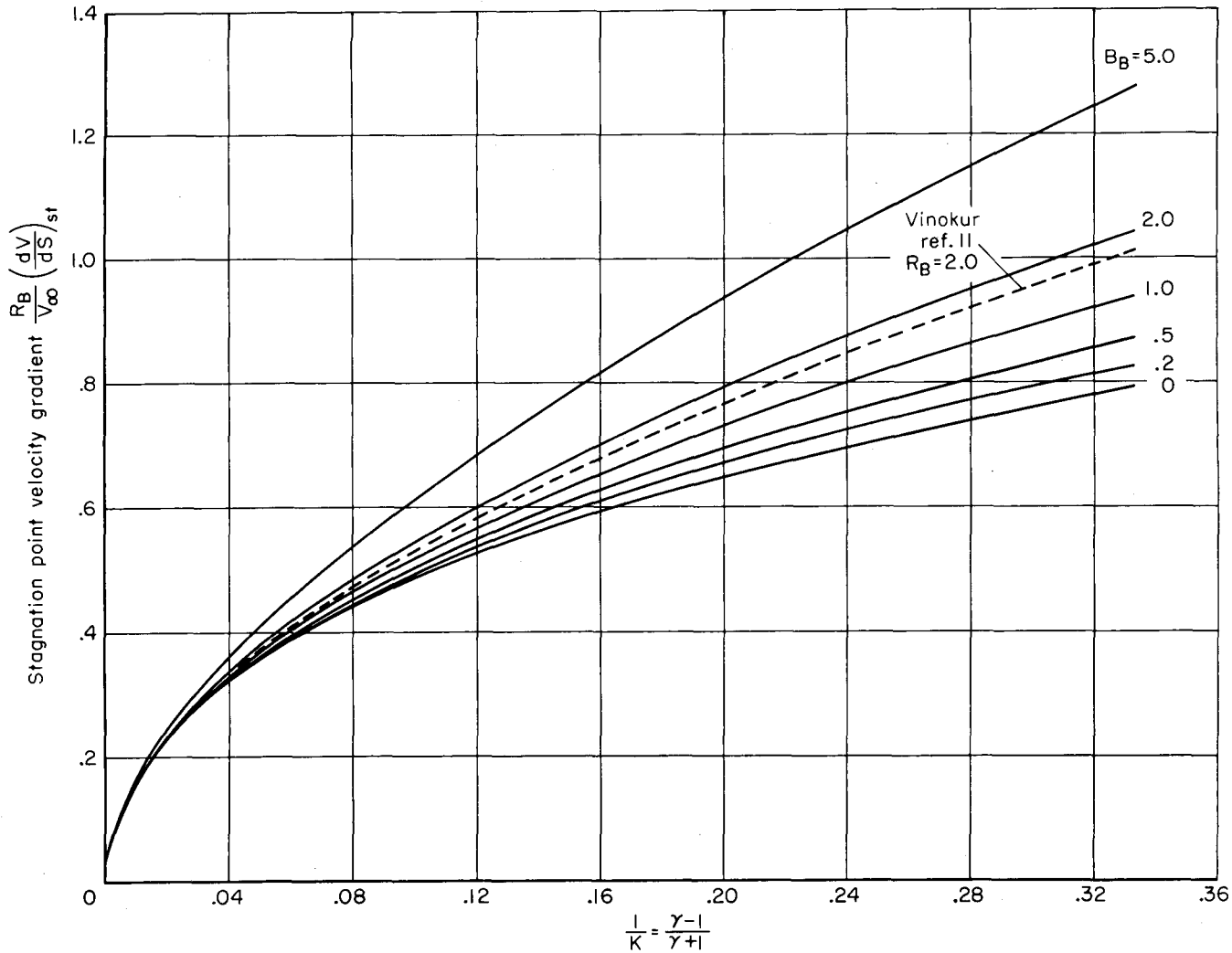

Figure 4.- Stagnation point velocity gradient at $M_\infty = \infty$ for several values of bluntness parameter, B_B.

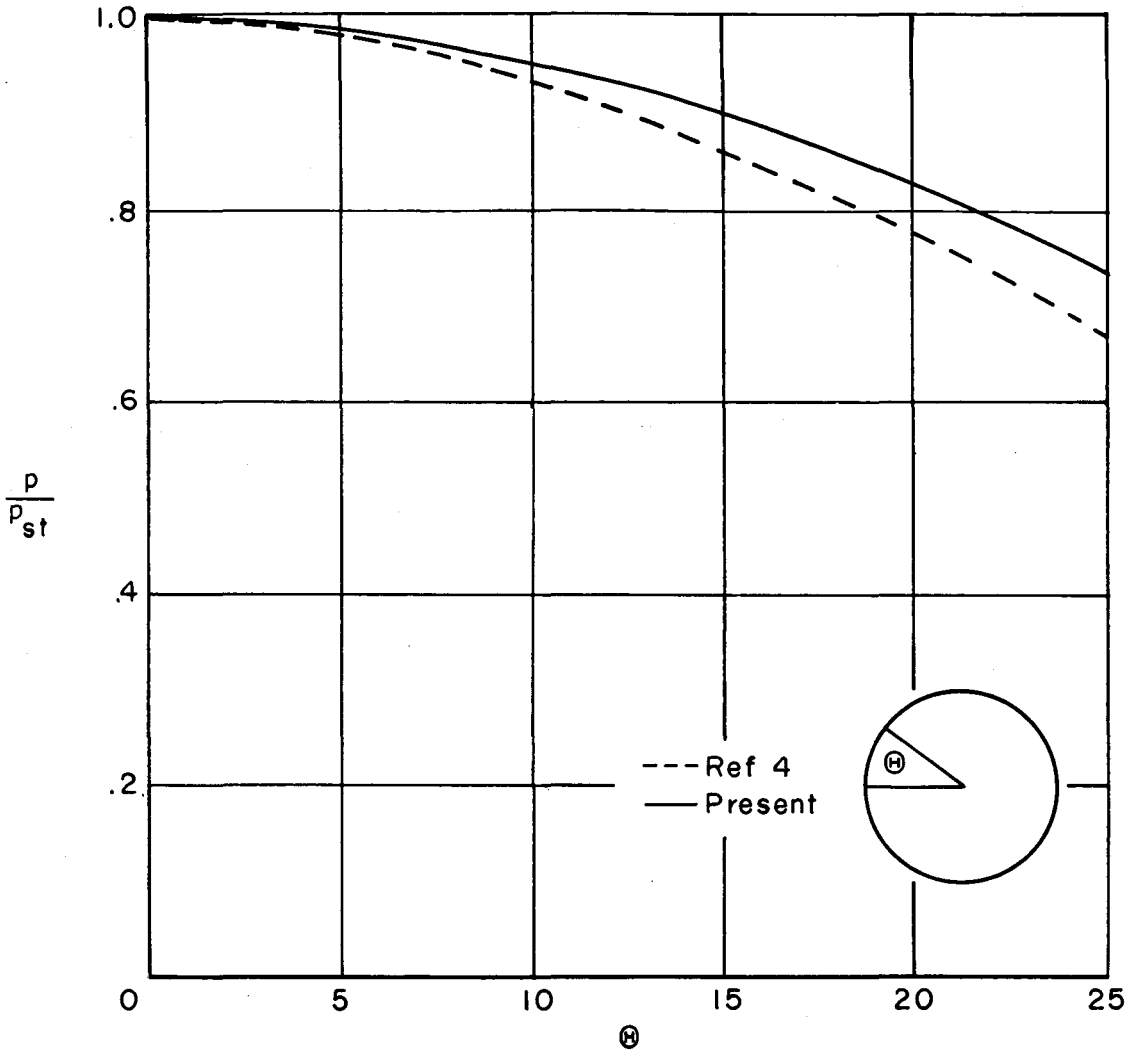

Figure 5.- Comparison of pressure distribution on a sphere for $\gamma = 1.4$ and $M_\infty = \infty$ with results of Van Dyke.

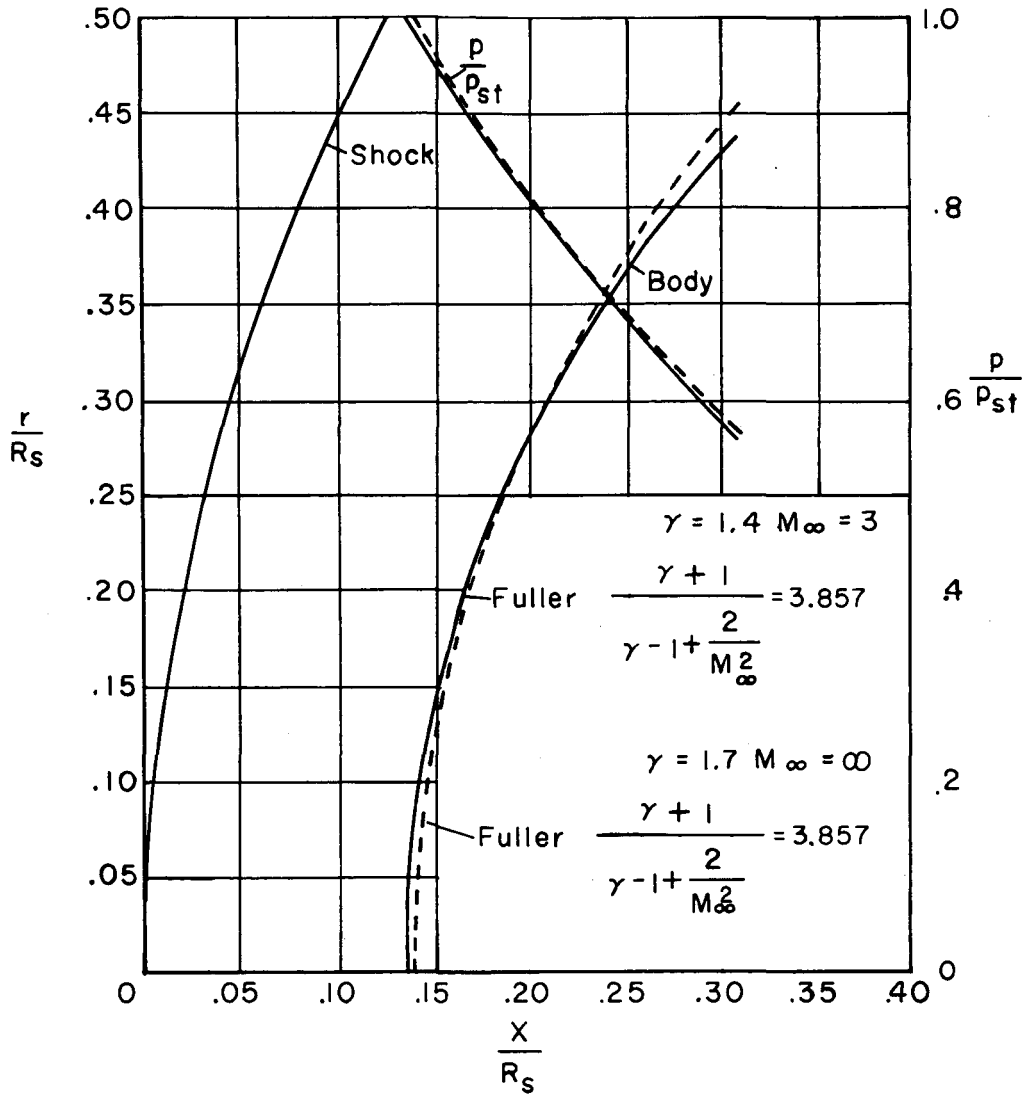

Figure 6.- A test of the validity of the similarity parameter; body shape and pressure distribution.

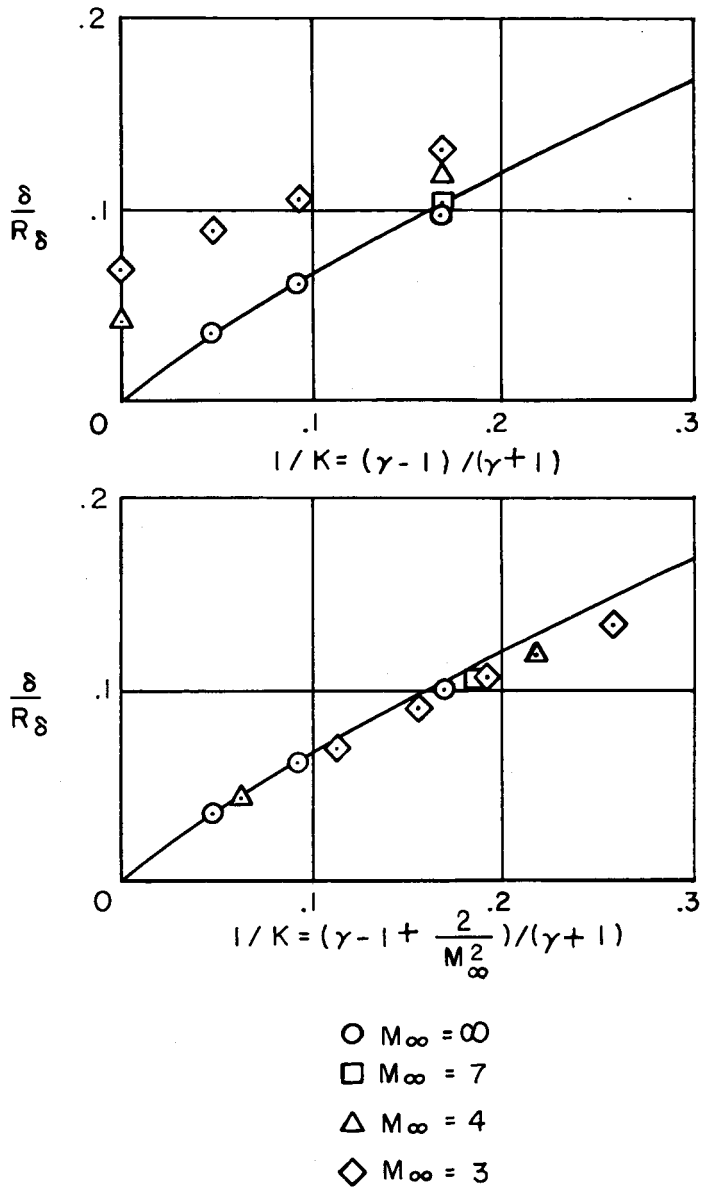

Figure 7.- A test of the validity of the similarity parameter; standoff distance.